Inorg. Chem. **2003**, *42*, 1848–1856

Synthesis, Crystal Structures, and Magnetic Properties of Two Cyano-Bridged Tungstate(V)–Manganese(II) Bimetallic Magnets

You Song,[†,‡] Shin-ichi Ohkoshi,[†] Yoichi Arimoto,[†] Hidetake Seino,[§] Yasushi Mizobe,[§] and Kazuhito Hashimoto*[,†,‡]

Research Center for Advanced Science and Technology, The University of Tokyo, 4-6-1 Komaba, Meguro-ku, Tokyo 153-8904, Japan, Kanagawa Academy of Science and Technology, 4-6-1 Komaba, Meguro-ku, Tokyo 153-8904, Japan, and Institute of Industrial Science, The University of Tokyo, 4-6-1 Komaba, Meguro-ku, Tokyo 153-8505, Japan

Received August 20, 2002

The reaction of manganese acetate with octacyanotungastate in an aqueous solution of concentrated acetic acid gives two new three-dimensional cyano-bridged manganese(II)–tungstate(V) bimetallic assemblies, $[Mn^{II}_2(H_2O)_2(CH_3COO)][W^V(CN)_8]\cdot 2H_2O$ (**1**) (tetragonal space group *I*4/*mcm*, $a = b = 11.9628(9)$ Å, $c = 13.367(2)$ Å, and $Z = 4$) and $Cs^{I}_{0.5}Mn^{II}_2[W^V(CN)_8](CH_3CO_2)_{1.5}\cdot H_2O$ (**2**) (monoclinic space group *C*2/*c*, $a = 16.274(2)$ Å, $b = 22.948(6)$ Å, $c = 13.196(1)$ Å, $\beta = 128.040(6)°$, and $Z = 8$). In complex **1**, $W^V(CN)_8$ adopts a square antiprismatic geometry, and each CN group coordinates to the Mn^{II} ions forming W–Mn_4–W–Mn_4– ··· columnar linkages where four sites on the Mn^{II} ion with octahedral geometry are occupied by CN groups. The columns are parallel and interlock, yielding a network structure. Complex **2** contains two different coordination geometries for $W^V(CN)_8$, namely, square antiprismatic and dodecahedral. The columnar structures appear also in **2**, where the Mn^{II} ions in two different environments provide three and four coordinated sites to the CN groups. The columns are bridged by both dodecahedral $W^V(CN)_8$ groups and acetates. Cs ions were intercalated in the lattice by the formation of short attractive contacts with the acetates. The field-cooled magnetization, ac susceptibility, and the field dependence of magnetization measurements show that both **1** and **2** are ferrimagnets with ordering temperatures 40 and 45 K, respectively. The investigation of the magnetostructural correlation shows that the ferrimagnetic ordering in **1** and **2** are attributed to the dominant antiferromagnetic exchange pathways d_{z^2}(W)–$d_{x'y'}$(Mn) and $d_{x^2-y^2}$(W) – $d_{x'y'}$(Mn).

Introduction

Over the past decade, Prussian blue analogues[1] involving hexacyanometalate $[M(CN)_6]^{n-}$ with 3d magnetic ions and polyhexacyanometalates containing organic ligands[2] have occupied a special position in the design and synthesis of new molecular based magnets due to their high critical temperatures and interesting functionalities such as photo-induced magnetism.[3] Today, synthetic chemists do not restrict the choice of magnetic cyanides to hexacyanometalates. In recent years, polycyanides with higher coordination numbers have attracted increasing interest. For example, Kahn's group first extended the Prussian blue system to study anisotropic magnetic effects using bimetallic cyanides of heptacyanomolybdate $[Mo(CN)_7]^{4-}$.[4] Conversely, our group in parallel with Decurtins' group[5,6] has prepared high-spin

* To whom correspondence should be addressed. E-mail: kazuhito@fchem.chem.t.u-tokyo.ac.jp

[†] Research Center for Advanced Science and Technology.

[‡] Kanagawa Academy of Science and Technology (KAST).

[§] Institute of Industrial Science.

(1) (a) Mallah, T.; Thiébaut, S.; Verdaguer, M.; Veillet, P. *Science* **1993**, *262*, 1554. (b) Verdaguer, M.; Mallah, T.; Gadet, V.; Castro, I.; Hélary, C.; Thiébaut, S.; Veillet, P. *Conf. Coord. Chem.* **1993**, *14*, 19. (c) Entley, W. R.; Girolami, G. S. *Science* **1995**, *268*, 397. (d) Ferlay, S.; Mallah, T.; Ouahès, R.; Veillet, P.; Verdaguer, M. *Nature* **1995**, *378*, 701. (e) Sato, O.; Iyoda, T.; Fujishima, A.; Hashimoto, K. *Science* **1996**, *271*, 49. (f) Buschmann, W. E.; Paulson, S. C.; Wynn, C. M.; Girtu, M. A.; Epstein, A. J.; White, H. S.; Miller, J. S. *Adv. Mater.* **1997**, *9*, 645. (g) Ohkoshi, S.; Hashimoto, K. *Chem. Phys. Lett.* **1999**, *314*, 210. (h) Ohkoshi, S.; Abe, Y.; Fujishima, A.; Hashimoto, K. *Phys. Rev. Lett.* **1999**, *82*, 1285. (i) Verdaguer, M.; Bleuzen, A.; Marvaud, V.; Vaissermann, J.; Seuleiman, M.; Desplanches, C.; Scuiller, A.; Train, C.; Garde, R.; Gelly, G.; Lomenech, C.; Rosenman, I.; Veillet, P.; Cartier, C.; Villain, F. *Coord. Chem. Rev.* **1999**, *190*, 1023. (j) Holmes, S. M.; Girolami, G. S. *J. Am. Chem. Soc.* **1999**, *121*, 5593. (k) Hatlevik, Ø.; Buschmann, W. E. Zhang, J.; Manson, J. L.; Miller, J. S. *Adv. Mater.* **1999**, *11*, 914. (l) Ohkoshi, S.; M. Mizuno, G.-j. Hung, Hashimoto, K. *J. Phys. Chem.* **2000**, *104*, 9365.

10.1021/ic025959x CCC: $25.00
Published on Web 02/28/2003

clusters from the assembly of octacyanometalates $[M(CN)_8]^{3-}$ ($M = Mo^V$, W^V).

Octacyanometalates $[M(CN)_8]^{n-}$ (M = Mo, W, ...) are a versatile class of building blocks that can adopt three different spatial configurations (e.g., square antiprism (D_{4h}), dodecahedron (D_{2d}), bicapped trigonal prism (C_{2v})), depending on their chemical environment, such as the surrounding ligands and the choice of metal ion.[7] Thus, a variety of coordination geometries can be found in the crystal structure of their complexes, i.e., zero-dimensional (0D),[5,6,8,9] 1D,[10,11] 2D,[12,13] and 3D.[14−18] In fact, the magnetic properties of these materials can be modulated by just these flexible molecular structures. In recent studies, we have observed drastic changes in the magnetic properties and the dimensionality of the structures by introducing different $[M(CN)_8]^{3-}$ geometries, e.g., 0D Mn_9W_6 cluster[5] with a bicapped trigonal prismatic $[M(CN)_8]^{3-}$ precursor and a 3D Mn_6W_4 complex[15] assembled from both bicapped trigonal prismatic and dodecahedral $[M(CN)_8]^{3-}$ precursors.

During the course of study, the structure and magnetic properties of novel manganese(II)−tungstate(V) polycyanides have been investigated. In previous work, we have demonstrated that the reacting media can effectively tune the structures of the products in this system.[5,15] On the basis of this knowledge, we have attempted to introduce acetic acid into the coordination reaction in order to utilize the competition between H^+ and acetic anions to control the reaction yielding different products. This paper details our extensive work on the syntheses and X-ray structures of two 3D bimetallic assemblies containing manganese Mn^{II} ions and the octacyanotungstate precursor $[W(CN)_8]^{3-}$. Moreover, the magnetic properties are determined from single crystals, and the magnetism of these cyano-bridged complexes containing 5d species is discussed.

Experimental Section

Materials. All chemicals are commercially available, and reagent grade products were used without purification. $Cs_3[W(CN)_8]\cdot 2H_2O$ was prepared according to the literature.[19]

Caution! Although no problems were encountered in the preparation of the following complexes, in acidic reaction conditions, suitable precautions should be taken when handling potentially poisonous compounds. It is of the utmost importance that all preparations be performed and stored in well-ventilated areas.

Preparation of $[Mn_2(H_2O)_2(CH_3CO_2)][W(CN)_8](H_2O)_2$ (1). A 2 mL portion of an aqueous solution containing cesium octacyanotungstate(V) dihydrate (137 mg, 0.167 mmol) was added to 3 mL of a stirred aqueous acetic acid solution (glacial acetic acid/water = 1:2 v/v) of manganese(II) acetate tetrahydrate (123 mg, 0.5 mmol). Then with constant stirring, an additional portion of glacial acetic acid (5 mL) was added dropwise. The resulting brown-yellow solution was left in the dark at room temperature for several days, and dark brown square prismatic crystals (**1**) were obtained together with a small amount of rhomboid plate crystals as the byproduct. This procedure afforded 74 mg of **1** and gave a percent yield of 73%. Single crystals of **1** suitable for X-ray crystallography were grown by slow diffusion in a test tube with manganese(II) acetate tetrahydate solid (125 mg, 0.5 mmol) in 15 mL of glacial acetic acid as the bottom layer and 2 mL of the aqueous solution containing cesium octacyanotungstate(V) dihydrate (165 mg, 0.2 mmol) as the top layer. Anal. Calcd for $C_{10}H_{11}N_8O_6Mn_2W$ (**1**): C, 18.98; H, 1.75; N, 17.70. Found: C, 18.96; H, 1.68; N, 17.68.

Preparation of $Mn_2Cs_{0.5}[W(CN)_8](CH_3CO_2)_{1.5}(H_2O)$ (2). Complex **2** was prepared by the same procedure described above from the following compounds, added dropwise: 3 mL of an aqueous acetic acid solution (glacial acetic acid/water = 1:2 v/v) of manganese(II) acetate tetrahydrate (367 mg, 1.5 mmol), 2 mL of an aqueous solution of cesium octacyanotungstate(V) dihydrate (414 mg, 0.5 mmol), and 11 mL of glacial acetic acid. After 9 h, **2** was obtained as dark brown rhomboidal plates in a yield of 291 mg, 86%. Single crystals of **2** suitable for X-ray crystallography could be picked from the products. Anal. Calcd for $C_{11}H_{6.5}N_8O_4Mn_2WCs_{0.5}$ (**2**): C, 19.58; H, 0.97; N, 16.60. Found: C, 19.52; H, 1.08; N, 16.63.

Crystallographic Data Collection and Structure Determination. The crystallographic data for complexes **1** and **2** are listed in Table 1.

A brown prismatic crystal of **1** measuring 0.30 × 0.2 × 0.15 mm and a brown plate crystal of **2** measuring 0.30 × 0.30 × 0.05 mm were mounted inside glass capillaries. All measurements were carried out using a Rigaku AFC7R diffractometer with graphite monochromated Mo Kα radiation and a rotating anode generator. The data were collected at a temperature of 25 ± 1 °C, using the $\omega-2\theta$ scanning technique with the maximum 2θ values of 54.9 ° for **1** and 55.0° for **2**. Scans of (1.68 + 0.30 tan θ)° for **1** and (1.05 + 0.30 tan θ)° for **2** were made at a speed of 16.0°/min (in ω).

Of the 1003 reflections that were collected, 612 were unique ($R_{int} = 0.012$) for **1**, and of the 5453 reflections, 4444 were unique

(2) (a) Ohba, M.; Usuki, N.; Fukita, N.; Õkawa; H. *Angew. Chem., Int. Ed.* **1999**, *38*, 1795. (b) Ohba, M.; Õkawa, H. *Coord. Chem. Rev.* **2000**, *198*, 313.

(3) (a) Sato, O.; Iyoda, T.; Fujishima, A.; Hashimoto, K. *Science* **1996**, *272*, 704. (b) Ohkoshi, S.; Yorozu; S.; Sato, O.; Iyoda, T.; Fujishima, K.; Hashimoto, K. *Appl. Phys. Lett.* **1997**, *70*, 1040. (c) Sato, O.; Einaga, Y.; Fujishima, A.; Hashimoto, K. *Inorg. Chem.* **1999**, *38*, 4405.

(4) (a) Larionova, J.; Clérac, R.; Sanchiz, J.; Kahn, O.; Golhen, S.; Ouahab, L. *J. Am. Chem. Soc.* **1998**, *120*, 13088. (b) Larionova, J.; Kahn, O.; Gohlen, S.; Ouahab, L.; Clérac, R. *J. Am. Chem. Soc.* **1999**, *121*, 3349−3356.

(5) Zhong, Z. J.; Seino, H.; Mizobe, Y.; Hidai, M.; Fujishima, A.; Ohkoshi, S.; Hashimoto, K. *J. Am. Chem. Soc.* **2000**, *122*, 2952.

(6) Larionova, J.; Gross, M.; Pilkington, M.; Andres, H.; Stoeckli-Evans, H.; Güdel, H. U.; Decurtins, S. *Angew. Chem., Int. Ed.* **2000**, *39*, 1605.

(7) Leipoldt, J. G.; Basson, S. S.; Roodt, A. *Adv. Inorg. Chem.* **1993**, *40*, 241.

(8) Sieklucka, B.; Szklarzewicz, J.; Kemp, T. J.; Errington, W. *Inorg. Chem.* **2000**, *39*, 5156.

(9) Podgajny, R.; Desplanches, C.; Sieklucka, B.; Sessoli, R.; Villar, V.; Paulsen, C.; Wernsdorfer, W.; Dromzee, Y.; Verdaguer, M. *Inorg. Chem.* **2002**, *41*, 1323.

(10) Rombaut, G.; Golhen, S.; Ouahab, L.; Mathoniere, C.; Kahn, O. *J. Chem. Soc., Dalton Trans.* **2000**, 3609.

(11) Li, D.; Gao, S.; Zheng, L.; Tang, W. *J. Chem. Soc., Dalton Trans.* **2002**, 2805

(12) Podgajny, R.; Korzeniak, T.; Balanda, M.; Wasiutynski, T.; Errington, W.; Kemp, T. J.; Alcock, N. W.; Sieklucka, B. *Chem. Commun.* **2002**, *10*, 1138.

(13) Arimoto, Y.; Ohkoshi, S.; Zhong, Z. J.; Seino, H.; Mizobe, Y.; Hashimoto, K. *Chem. Lett.* **2002** 832.

(14) Garde, R.; Desplanches, C.; Bleuzen, A.; Veillet, P.; Verdaguer, M. *Mol. Cryst. Liq. Cryst.* **1999**, *334*, 587.

(15) Zhong, Z. J.; Seino, H.; Mizobe, Y.; Hidai, M.; Verdaguer, M.; Ohkoshi, S.; Hashimoto, K. *Inorg. Chem.* **2000,** *39*, 5095.

(16) Meske, W.; Babel, D. *Z. Anorg. Allg. Chem.* **1999**, *625*, 51.

(17) Sra, A. K.; Rombaut, G.; Lahitete, F.; Golhen, S.; Ouahab, L.; Mathoniere, C.; Yakhmi, J. V.; Kahn, O. *New J. Chem.* **2000**, *24*, 871.

(18) Li, D.-F.; Gao, S.; Zheng, L.-M.; Sun, W.-Y.; Okamura, T.; Ueyama, N.; Tang, W.-X. *New J. Chem.* **2002**, *26*, 485.

(19) Bok, L. D. C.; Leipoldt, J. G.; Basson, S. S. *Z. Anorg. Allg. Chem.* **1975**, *415*, 81.

Table 1. Data Collection and Crystallographic Parameters for **1** and **2**

cpd	1	2
emp form.	$C_{10}H_{11}N_8O_6Mn_2W$	$C_{11}H_{6.50}N_8O_4Mn_2Cs_{0.50}W$
fw	632.97	674.90
cryst syst	tetragonal	monoclinic
space group	*I*4/*mcm*	*C*2/*c*
a / Å	11.96289(9)	16.274(2)
b / Å		22.948(6)
c / Å	13.367(2)	13.196(1)
β /deg		128.040(6)
V / Å^3	1912.9(3)	3881.4(1)
Z	4	8
D_{calc}/g·cm^{-3}	2.198	2.310
μ(Mo Kα)/cm^{-1}	73.49	81.58
λ/Å	0.71069	0.71069
no. obsvs (I > 3.00σ(I))	831	4532
no. of variables	49	288
R_1; wR_2[a]	0.015; 0.051	0.035; 0.110
GOF on F^2	0.97	1.05

[a] $R_1 = \sum ||F_o| - |F_c|| / \sum |F_o|$; $wR_2 = [\sum(w(F_o^2 - F_c^2)^2) / \sum w(F_o^2)^2]^{1/2}$.

($R_{int} = 0.036$) for **2**. The intensities of three representative reflections were measured every 150 reflections. Decay corrections were not applied. The empirical absorption corrections based on azimuthal scans of several reflections were applied, which resulted in transmission factors ranging from 0.87 to 1.00 for **1** and 0.33 to 1.00 for **2**. The data were corrected for Lorentz and polarization effects. The structures were solved by direct methods and expanded using Fourier techniques.[20] Non-hydrogen atoms were anisotropically refined. Hydrogen atoms were isotropically refined in complex **2**. All calculations were performed using the CrystalStructure crystallographic software package.[21]

Physical Measurements. Elemental analyses were carried out by standard microanalytical methods. The infrared spectra were recorded on a Shimadzu FT-IR 8200PC spectrometer with a paraffin suspension in the 4000−400 cm^{-1} region. X-ray diffraction (XRD) data for all crystalline samples were collected using a Rigaku Miniflex diffractometer. Magnetization measurements were carried out with a Quantum Design MPMS-5S superconducting quantum interference device (SQUID) magnetometer, working under an applied field of up to 50 kG.

Results and Discussion

Synthesis. In general, coordination reactions usually occur in a neutral or a slightly alkaline medium rather than an acidic one, because the latter gives rise to lower electronic density of the donor atoms on the ligands, rendering most ligands unreactive with regards to the coordination of metal ions. In neutral or slightly alkaline solutions, however, controlling the reaction speed is difficult and the growth of single crystals of suitable size for study in some reactions can be a challenge. This problem is more outstanding in synthesizing cyano-bridged systems. Another problem with the use of octacyanometalate(V) precursors is that $[W^V(CN)_8]^{3-}$ is easily reduced into $[W^{IV}(CN)_8]^{4-}$ in alkaline or neutral solutions. In contrast, when acetic acid (HAc) is the reaction

Scheme 1

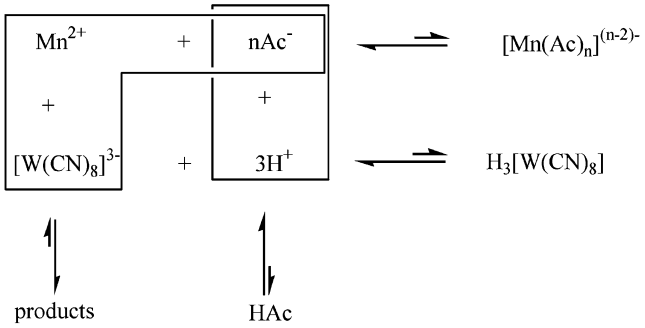

medium, the Ac$^-$ ions prevent free metal ions such as Mn^{2+} from reacting with $[W^V(CN)_8]^{3-}$, and the H^+ ions protect the $[W^V(CN)_8]^{3-}$ precursor by forming $H_3[W^V(CN)_8]$ as shown in Scheme 1. Thus, the yield of products can be changed, depending on the concentration of HAc, and the single crystals can be obtained by controlling the reaction speed.

$MnAc_2 \cdot 4H_2O$ reacted with $Cs_3[W(CN)_8] \cdot 2H_2O$ to form a brown precipitate in aqueous solution (pH $\sim$ 4). When one drop of HAc was added before reaction, no precipitate was observed in the solution (pH $\sim$ 3) because the effect of the H^+ ions weakened the ability of $[W^V(CN)_8]^{3-}$ to coordinate to Mn^{2+}. In fact, when the concentration of Ac$^-$ ions was low ($V_{acid}/V_{water} \leq 0.75$), H^+ was the major factor in controlling this reaction. Increasing the concentration of HAc higher than $V_{acid}/V_{water} = 1$ led to enough Ac$^-$ ions for product formation, but the increase in H^+ concentration effectively reduced the reaction speed. The competition between retarding and accelerating the reaction from H^+ and Ac$^-$ was clearly observed in experiments in Table 2. The reaction was sped up as the concentration of HAc increased. The products of either **1** or **2** could also be controlled by altering the concentration of HAc. The experiments showed that **2** as the main product was formed at lower concentration of HAc. When the concentration of HAc was between $1.5 \leq V_{acid}/V_{water} < 2.5$, **1** would be the main product rather than **2**, and the well-shape crystals were grown in an optimum V_{acid}/V_{water} ratio = 2. In the range of high concentration of HAc, $V_{acid}/V_{water} \geq 3$, only **2** was observed. In general, adjusting the concentration of H^+ and Ac$^-$ ions played an important role in controlling the self-assembly of the reactants into different products.

IR Spectrum. The IR spectrum of complex **1** showed a sharp CN stretch, ν(CN) = 2176.5 cm^{-1}, indicating that the cyano groups of $W(CN)_8$ were chemically equivalent. The CN stretch was higher than those of $Cs_3[W^V(CN)_8] \cdot 2H_2O$ (ν(CN) = 2150 and 2136.5 cm^{-1}), suggesting that the CN groups bridge the Mn^{II} and W^V metal ions.[1d,22] For complex **2**, three sharp peaks ν(CN) = 2181.3, 2150.5, and 2109.5 cm^{-1} along with shoulders at 2156.3 and 2118.2 cm^{-1} were observed, indicating the presence of more than five crystallographically inequivalent CN groups. The X-ray structure for **2,** described as following, is in agreement with this result.

(20) *DIRDIF99*: Beurskens, P. T.; Admiraal, G.; Beurskens, G.; Bosman, W. P.; de Gelder, R.; Israel, R.; Smits, J. M. M. 1999. The DIRDIF-99 program system, Technical Report of the Crystallography Laboratory, University of Nijmegen, The Netherlands.

(21) *CrystalStructure 2.00*: *Crystal Structure Analysis Package*, Rigaku and MSC 2001. *CRYSTALS Issue 10*: Watkin, D. J.; Prout, C. K.; Carruthers, J. R.; Betteridge, P. W. Chemical Crystallography Laboratory, Oxford, UK.

(22) Hatlevik, Ø; Buschmann, W. E.; Zhang, J.; Manson, J. L.; Miller, J. S. *Adv. Mater.* **1999**, *9*, 645.

Table 2. Expermental Conditions for the Crystallization of Complexes **1** and **2**

HAc:H_2O (V:V)[a]	product[b]	time	method
≤0.75	no crystals or precipitate	2 weeks	evaporation
1	hexagonal plate crystals of **2** and a small amount of **1**[c]	1 week	evaporation
2 (1.5−2.5)	well-formed square prism crystals of **1** and a very small amount of **2**	3 days	evaporation
2.5	square prismatic crystals of **1** and rhomboidal crystals of **2**	14 hours	evaporation
≥3	poorly shaped plate crystals or microcrystallines of **2**	9 hours	diffusion

[a] The solutions contain 0.5 mmol of $MnAc_2 \cdot 4H_2O$ and 0.167 mmol of $Cs_3[W(CN)_8] \cdot 2H_2O$, and the total volumes range from 7 to 16 mL. [b] All synthetic procedures were reproducible, but the ratios of **1** and **2** could not be completely the same in every experiment. [c] **1** and **2** in all reactions can be separated by hand, and XRD spectra showed that the hexagonal crystals, rhomboid crystals, and microcrystals were all **2**.

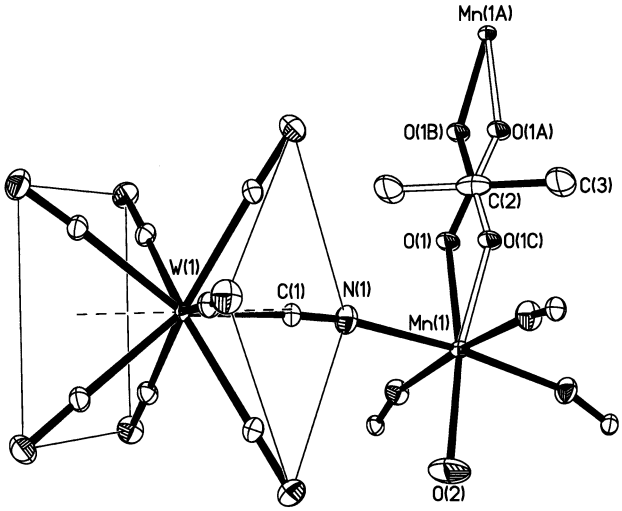

Figure 1. ORTEP drawing of the coordination environments around the W^V and Mn^{II} ions for complex **1**. Displacement ellipsoids are drawn at a 30% probability level. The dashed line around W(1) is the quasi-$\bar{8}$-axis for square antiprism $W(CN)_8$. Hydrogen atoms and a free water molecule have been omitted for clarity.

Table 3. Selected Bond Lengths (Å) and Angles (deg) for **1**

Bond Lengths

W(1)	C(1)	2.163(2)	Mn(1)	O(1)	2.084(5)
Mn(1)	O(2)	2.187(5)	Mn(1)	N(1)	2.248(2)
O(1)	C(2)	1.155(5)	N(1)	C(1)	1.143(3)
C(2)	C(3)	1.568(9)			

Bond Angles

O(1)	Mn(1)	O(2)	169.6(1)	O(1)	Mn(1)	N(1)	86.0(1)
O(2)	Mn(1)	N(1)	86.80(6)	Mn(1)	O(1)	C(2)	150.6(3)
Mn(1)	N(1)	C(1)	165.4(2)	W(1)	C(1)	N(1)	177.1(2)
O(1)	C(2)	C(3)	109.02				

The band at 2109.5 cm^{-1} is different from that of $K_4[W^{IV}(CN)_8]$ around 2100 cm^{-1}. The latter usually reveals a broad band 2050−2110 cm^{-1} with the high intensity. For comparison, $Mn_2[W^{IV}(CN)_8] \cdot 8H_2O$ as a reference was mixed into **2** in a same percentage of CN and then the IR spectra of the mixture was recorded. The result showed a broad band 2070−2160 cm^{-1} with two shoulders from $[W^{IV}(CN)_8]^{4-}$, and the intensity is four times greater than the strongest band from **2**.

Crystal Structure of 1. The structure of **1** shows that this compound crystallizes in tetragonal space group *I*4/*mcm* and is composed of three-dimensional $[Mn^{II}_2(H_2O)_2(CH_3CO_2)][W^V(CN)_8]$ networks containing two water molecules, as shown in Figure 1. Selected bond lengths and angles are listed in Table 3. $W^V(CN)_8$ adopts a square antiprism geometry, in which all angles between the W−CN and the quasi-8-axis (the dash line around W(1) in Figure 1) are 57.4°

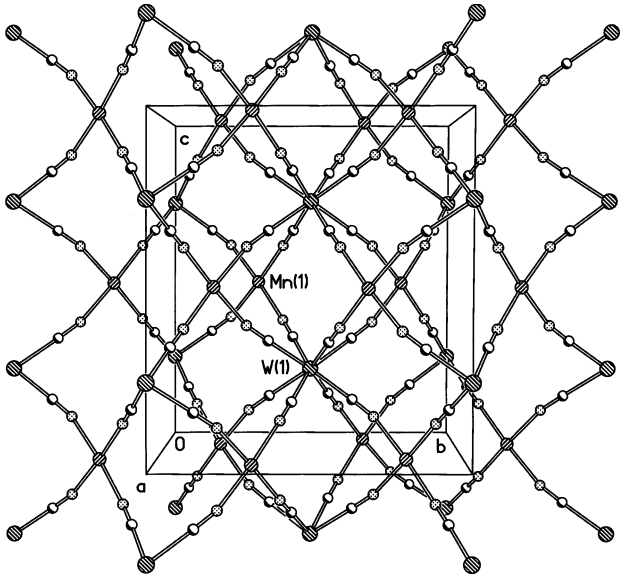

Figure 2. Projection showing the 3D $\{Mn^{II}_2[W^V(CN)_8]\}_n$ networks for complex **1** viewed down the *a* axis.

and all edge lengths of the polyhedron are 1.191 times the distance of the W−CN bond, comparable with those of the most favorable polyhedron (MFP) of square antiprism (57.1° and 1.2156 times).[7] Each CN group of $W^V(CN)_8$ is coordinated to eight Mn^{II} ions, giving rise to a $W-Mn_4-W-Mn_4-\cdots$ columnar linkage (Figure 2). The bond angles of W(1)−C(1)−N(1) and Mn(1)−N(1)−C(1) are 177.1(2) and 165.4(2)°, respectively, and the torsion angle of W(1)−C(1)−N(1)−Mn(1) is −27.3(5)°, which are all comparable with the previously reported three-dimensional W^V-Mn^{II} compound.[15] All of the columns interlock with each other to form the skeleton of the three-dimensional structure, as shown in Figure 2. The Mn^{II} ions are located in the center of a distorted octahedron $Mn(NC)_4(H_2O)(CH_3CO_2)$, where the four N atoms of the CN groups are coplanar with Mn(1), while an acetate anion bridges between the two Mn^{II} centers at the apical position and an H_2O molecule binds trans to the acetate. $[W^V(CN)_8]$ groups bridge with the disordered acetate anions to connect to the Mn^{II} ions forming this three-dimensional network. The shortest distance between Mn^{II} and W^V ions is 5.499 Å, while that between two W^V ions is 6.683 Å. Residual water molecules occupy positions within the lattice.

Crystal Structure of 2. The surroundings around the metal ions and selected linkages between the metal ions of **2** are illustrated in Figure 3. Selected bond lengths, bond angles, and torsion angles are listed in Table 4. In this structure, there are two types of W^V centers and two types of Mn^{II}

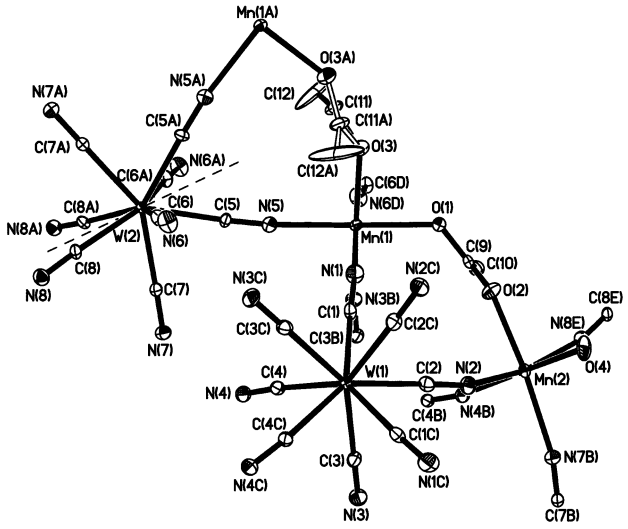

Figure 3. ORTEP drawing of the coordination environments around the W^V and Mn^{II} ions for complex **2**. Displacement ellipsoids are drawn at a 30% probability level. The dashed line around W(2) is the quasi-4-axis for dodecahedron $W(CN)_8$. Hydrogen and cesium atoms have been omitted for clarity. The symmetry codes are as follows: (A) $-x, y, {}^1/_2 - z$; (B) ${}^1/_2 + x, {}^1/_2 - y, -z$; (C) $-{}^1/_2 + x, {}^1/_2 - y, -{}^1/_2 + z$; (D) ${}^1/_2 + x, {}^1/_2 - y, {}^1/_2 + z$; (E) ${}^1/_2 + x, -{}^1/_2 + y, z$.

Table 4. Selected Bond Lengths (Å) and Angles (deg) for **2**[a]

Bond Lengths

W(1)	C(1)	2.139(6)	W(1)	C(2)	2.156(6)
W(1)	C(3)	2.166(6)	W(1)	C(4)	2.166(6)
W(2)	C(5)	2.164(6)	W(2)	C(6)	2.148(6)
W(2)	C(7)	2.177(6)	W(2)	C(8)	2.173(6)
Mn(1)	O(1)	2.160(5)	Mn(1)	O(3)	2.119(5)
Mn(1)	N(1)	2.224(5)	Mn(1)	N(5)	2.254(6)
Mn(2)	O(2)	2.183(5)	Mn(2)	O(4)	2.200(5)
Mn(2)	N(2)	2.225(6)	N(1)	C(1)	1.153(8)
N(2)	C(2)	1.147(8)	N(3)	C(3)	1.131(8)
N(4)	C(4)	1.140(8)	N(5)	C(5)	1.166(8)
N(6)	C(6)	1.148(8)	N(7)	C(7)	1.148(8)
N(8)	C(8)	1.130(8)			

Bond Angles

C(1)	W(1)	C(2)	73.9(2)	C(1)	W(1)	C(3)	113.2(2)
C(2)	W(1)	C(3)	72.0(2)	C(1)	W(1)	C(4)	73.8(2)
C(2)	W(1)	C(4)	116.1(2)	C(3)	W(1)	C(4)	72.5(2)
C(5)	W(2)	C(6)	81.2(2)	C(5)	W(2)	C(7)	71.1(2)
C(6)	W(2)	C(7)	92.5(2)	C(5)	W(2)	C(8)	133.3(2)
C(6)	W(2)	C(8)	69.8(2)	C(7)	W(2)	C(8)	74.5(2)
W(1)	C(1)	N(1)	177.2(6)	W(1)	C(2)	N(2)	178.8(6)
W(1)	C(3)	N(3)	179.0(6)	W(1)	C(4)	N(4)	175.5(5)
W(2)	C(5)	N(5)	174.3(5)	W(2)	C(6)	N(6)	176.4(6)
W(2)	C(7)	N(7)	176.9(6)	W(2)	C(8)	N(8)	177.4(5)
C(1)	N(1)	Mn(1)	161.8(6)	C(2)	N(2)	Mn(2)	157.4(5)
C(3)	N(3)	Mn(1B)	173.9	C(4)	N(4)	Mn(2B)	168.3
C(5)	N(5)	Mn(1)	171.3(6)	C(6)	N(6)	Mn(1C)	169.5
C(7)	N(7)	Mn(2B)	163.4	C(8)	N(8)	Mn(2F)	165.9

Torsion Angles

W(1)	C(1)	N(1)	Mn(1)	121.7(1)
W(1)	C(2)	N(2)	Mn(2)	97.3(3)
W(1)	C(3)	N(3)	Mn(1B)	−59.6
W(1)	C(4)	N(4)	Mn(2B)	−46.7
W(2)	C(5)	N(5)	Mn(1)	111.4(6)
W(2)	C(6)	N(6)	Mn(1C)	117.4
W(2)	C(7)	N(7)	Mn(2B)	−43.8
W(2)	C(8)	N(8)	Mn(2F)	160.7

[a] Symmetry code: (A) $-x, y, {}^1/_2 - z$; (B) ${}^1/_2 + x, {}^1/_2$-y, -z; (C) $-{}^1/_2 + x, {}^1/_2 - y, -{}^1/_2 + z$; (D) ${}^1/_2 + x, {}^1/_2 - y, {}^1/_2 + z$; (E) ${}^1/_2 + x, -{}^1/_2 + y, z$; (F) $-{}^1/_2 + x, {}^1/_2 + y, z$.

centers. The geometry around W(1) can be described as square antiprismatic, because the angles between the bonds

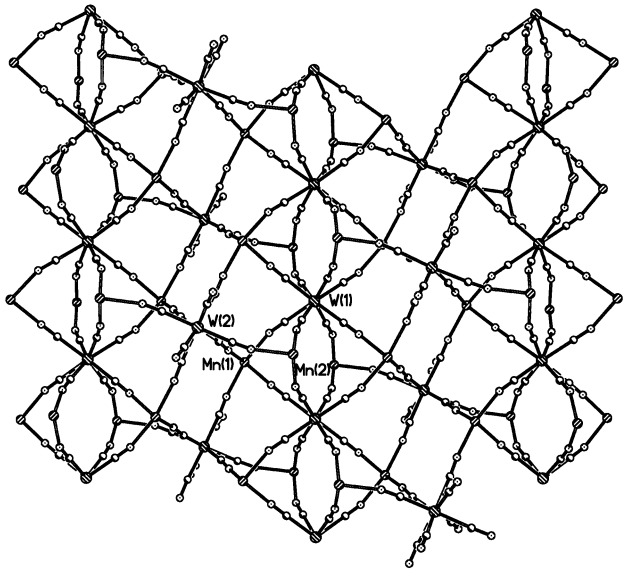

Figure 4. Projection of the structure of **2** viewed down the *b* axis. The linear $W(1)-Mn_4-W(1)-Mn_4-$ alternating columns run through the diagonal direction of *a* and *c* axes and are linked by $[W(2)(CN)_8]$ to form this 2D plane. Three facial sites of each Mn are occupied within the column.

of the W−CN and the quasi-$\bar{8}$-axis (C(1)C(2)C(3)C(4) as the basal plane) are 56.6 and 58.0°, respectively. The average value of edge lengths of the basal plane ranges from 2.539 to 2.562 Å and is 1.190 times that of all W−CN bond lengths, which range from 2.139(6) to 2.166(6) Å. The geometry around W(2), however, favors a dodecahedron. So, there exist two sets of symmetry-equivalent W(2)−C bonds (W(2)−C(i) i = 5, 5A, 8, 8A and W(2)−C(j) j = 6, 6A, 7, 7A), a quasi-4-axis (dash line in Figure 3) through W(2) and along the bisectors of angle C(8)W(2)C(8A) and C(5)W(2)C(5A) (symmetry code A: $-x, y, {}^1/_2 - z$), and four sets of different edges in it. The ratio of the two sets of symmetry-equivalent W(2)−C bond lengths is 1.00. The angles between this axis and W(2)−C(*i*) or W(2)−C(*j*) are 35.9 or 73.8°, respectively. All of these values are comparable with those of the MFP of a dodecahedron.[7] The four sets of edge lengths referred to as a unit length in an average W(2)−C distance are 1.19, 1.14, 1.29, and 1.28, respectively, and only the last shape parameter deviates from that of the MFP. The NC−W(2)−CN angles between neighboring C−W(2) bonds range from 69.8(2) to 92.5(2)°. All of angles N−C−W range from 175.5(5) to 179.0(6)°, which exhibits linear linkages close to 180° and highly delocalized electronic density between W^V ions and CN groups. All Mn^{II} ions are located in the center of distorted octahedral environments. Each CN group of $[W(1)(CN)_8]$ coordinates to Mn(1) and Mn(2) to form linear $W-Mn_4/W-Mn_4$ alternating columns along the diagonal direction of the *a* and the *c* axes ($\bar{8}$-axes) (Figure 4). The distance of the adjacent repeating units of W(1)···W(1B) (symmetry code B: ${}^1/_2 + x, {}^1/_2 - y, -z$) is 6.612 Å. The distances between W(1) and Mn^{II} ions are 5.455 Å for Mn(1)···W(1), 5.516 Å for Mn(1B)···W(1), 5.425 Å for Mn(2)···W(1), and 5.496 Å for Mn(2B)···W(1). All linkages between Mn^{II} ions and CN groups are not linear like those between W and CN. The bond angles of Mn−N−C range from 157.4(5) to 171.3(6)°, which are

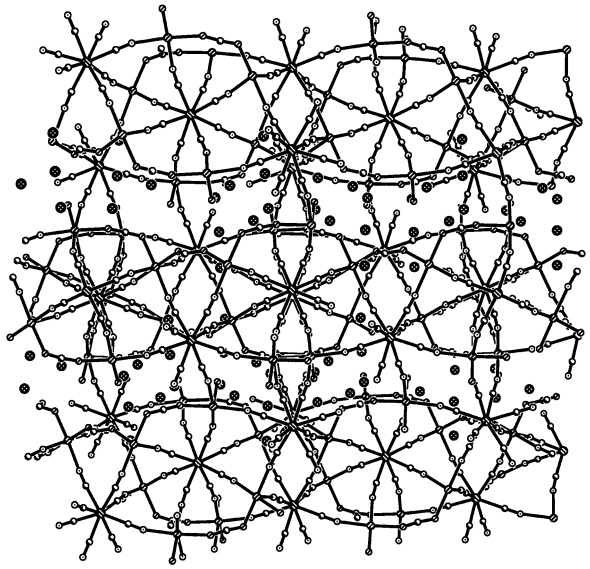

Figure 5. The 3D network for **2** formed by linking W(2) and Mn(2) in the planes shown in Figure 4. The view runs parallel to the *b* axis and along the diagonal direction of *a* and *c* axes. The crosshatched circles are the cesium atoms.

similar to those in other complexes of this type of system.[5,15] It is indicative of the flexibility of W−C−N−Mn linkages in $Mn^{II}-W^{V}(CN)_8$ system that may lead to the versatile structures of bimetallic octacyanides. Mn(1) and Mn(2) ions provide two sites, respectively, for linking within the chains and are meanwhile bridged by the acetates encircling the columns with Mn(1)···Mn(2) distances of 5.748 Å. The $(W-Mn_4)_n$ columns are linked to each other in the *ac* plane by [W(2)$(CN)_8$] groups and by the disordered acetates via the nearest Mn(1) or Mn(2) ions between neighboring columns, i.e., Mn(1)−W(2)−Mn(1), Mn(2)−W(2)−Mn(2) and Mn(1)−acetate−Mn(1). Here, [W(2)$(CN)_8$] provides six CN groups, all except C(8)N(8) and C(8A)N(8A), to complete the planar linkage (Figure 4). The distances from W(2) to Mn(1) and Mn(2) are W(2)···Mn(1) of 5.567 Å, W(2)···Mn(1C) of 5.524 Å (symmetry code C: $-{}^1/_2 + x$, ${}^1/_2 - y$, $-{}^1/_2 + z$), and W(2)···Mn(2B) of 5.557 Å, respectively, while the distance between the two Mn(1) ions bridged by acetate is 5.958 Å and is regarded as one of the shortest distances between metal ions of adjacent columns. Thus, these links complete the octahedral configuration by filling all sites of Mn(1). One vacant site still remains on Mn(2) after coordinating one H_2O molecule. The same [W(2)$(CN)_8$] groups also connect to the planes via C(8)N(8) and C(8A)N(8A), occupying the vacant site of Mn(2) ions within the neighboring plane to form the three-dimensional network. The distance between W(2) and Mn(2) is 5.498 Å. Cs ions are intercalated between the two planes and fixed in the lattice via electrostatic interactions with the oxygen donors of all the acetates (Figure 5).

Magnetic Properties of 1. Magnetic susceptibility (χ_M) measurements of the crystalline sample of **1** were carried out from 300 to 2 K (see Supporting Information). The effective magnetic moment (μ_{eff}) was 8.37 μ_B at room temperature, slightly less than the spin-only value of 8.54 μ_B for the two Mn^{II} ($3d^5$, $S = {}^5/_2$) ions and one W^{V} ($5d^1$, $S = {}^1/_2$) ion, suggesting an antiferromagnetic coupling between Mn^{II} and W^{V}. A single crystal of **1** was used for the measurements of the anisotropic magnetic effect along both the *ab* plane and the *c* axis. Field-cooling magnetization (FCM) curves revealed a long-range magnetic ordering of **1** below 40 K (Figure 6). ac susceptibility measurements were in agreement with this value. The field dependence on magnetization is shown in Figure 7a. The coercive field (H_c) was not observed in the *ab* plane, but along the *c* axis, a very small value of 9 Oe was observed in the inset of Figure 7b. All magnetic measurements of the single-crystal sample for **1** showed that there is an anisotropic effect for this complex. The magnetization value in the *ab* plane was about 2.78 times the value of that along the *c* axis at 2 K in Figure 6. The $M-H$ plot shows that the magnetization in the *ab* plane sharply increased and saturated (9.07 $N\beta$) around 2 kOe. The saturation of the magnetization along the *c* axis was observed at 4 kOe, indicating that the easy axis of magnetization is in the *ab* plane. The observed magnetic anisotropy of **1** may be attributed to the structural anisotropy. The magnetization saturation value of 9 $N\beta$ is identical with the antiferromagnetically coupled value of WMn_2 (W^{V}: $5d^1$, $S = {}^1/_2$; Mn^{II}: $3d^5$, $S = {}^5/_2$) ions, showing the ferrimagnetic nature of complex **1**.

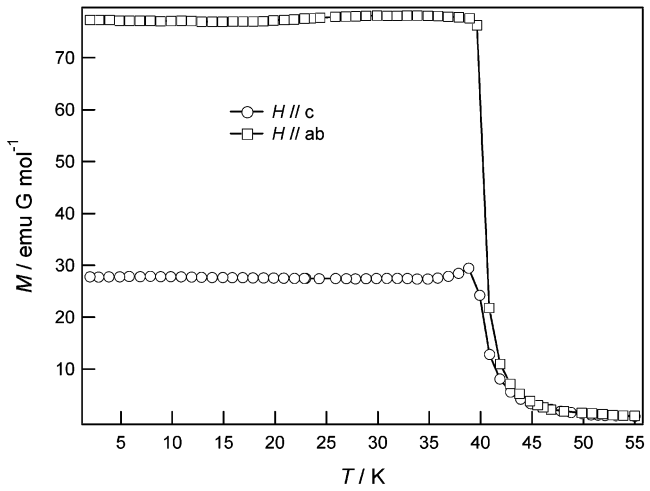

Figure 6. FCM measurement for complex **1** in the *ab* plane and the *c* axis, respectively. The applied field is 1 Oe.

Magnetic Properties of Complex 2. The observed μ_{eff} value of 7.99 μ_B for **2** at room temperature was also less than the spin only value of 8.54 μ_B. The field-cooling magnetization curve under an external field of 5 Oe (FCM) showed a long-range magnetic ordering of this ferrimagnet below 45 K (Figure 8). Figure 9 shows the field dependence of magnetization. At low fields, the magnetization sharply increased and reached to saturation at approximately 35 kOe. The value of 9.05 $N\beta$ at 50 kOe is close to the expected spontaneous magnetization of 9 $N\beta$ for the antiparallel ordering of unpaired electrons of WMn_2, indicating that **2** is a ferrimagnet.

Superexchange Pathways of Ferrimagnets 1 and 2. The magnetic orbitals coupling between Mn^{II} and W^{V} will be discussed to understand the magnetism of these complexes. In the present system, one unpaired electron and five

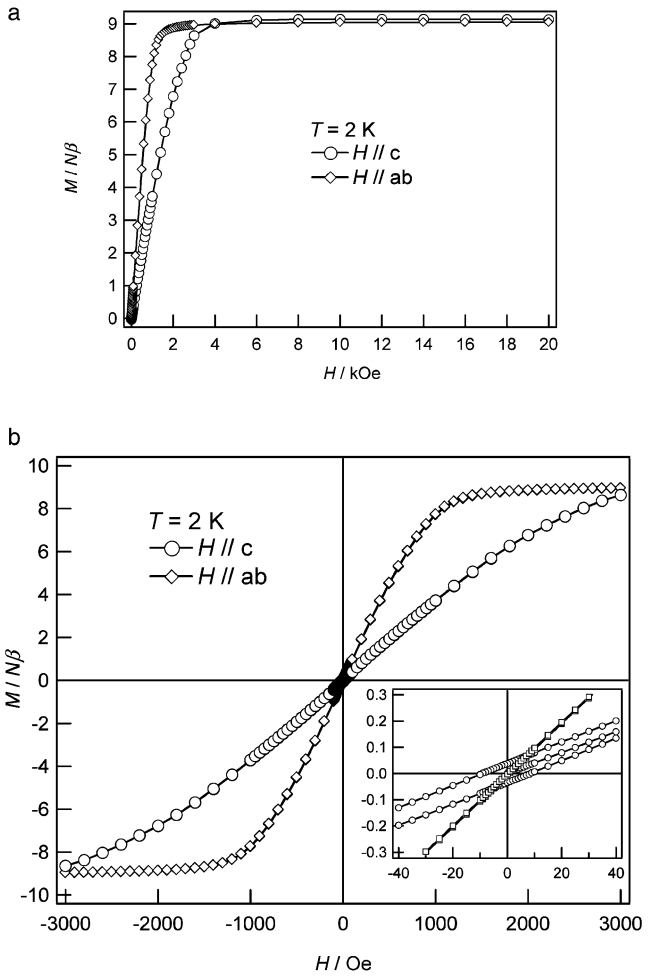

Figure 7. Field dependence of the magnetization (a) and hysteresis (b) of complex **1** in the *ab* plane and the *c* axis, respectively. Inset is the enlarged $M-H$ plot in the range of −40 to 40 Oe (see the text).

unpaired electrons are occupied on W^V and Mn^{II} metal ions, respectively. The exchange interaction parameters (J) can be expressed by eq 1:[23]

$$J = \frac{1}{n_A n_B} \sum_{\mu=1}^{n_A} \sum_{\nu=1}^{n_B} J_{\mu\nu} \qquad (1)$$

For W^V-Mn^{II}, the eq 1 can be described as follows:

$$J_{MnW} = \frac{1}{5}(J_{11} + J_{12} + J_{13} + J_{14} + J_{15}) \qquad (2)$$

The local $W^V(CN)_8$ structure of **1** shows a D_{4d} symmetry describing a square antiprism and $Mn^{II}(NC)_4O_2$ shows a D_{4h} symmetry. Assuming that all W−C−N−Mn links are linear, the molecule, $O_2(CN)_3Mn-NC-W(CN)_7$, in **1** shows approximately C_s symmetry, where a mirror can be drawn through x', y', and z axes (Figure 10). When $W^V(CN)_8$ and $Mn^{II}(NC)_4O_2$ are placed in C_s symmetry, the molecular orbital energy levels and symmetrical modes are shown in Scheme 2.[24−26] The expected superexchange pathways among the occupied molecular orbitals are shown in Figure 10. The d_{z^2} orbital of $W^V(CN)_8$ and the $d_{x'z'}$ and $d_{y'z'}$ orbitals of Mn^{II} result

(23) Kahn, O. *Molecular Magnetism*; VCH: New York, 1993; p 187.

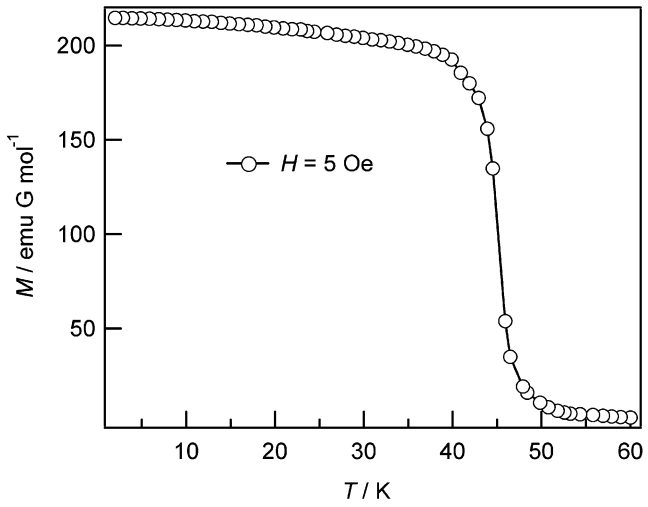

Figure 8. FCM measurement for complex **2**. The applied field is 5 Oe.

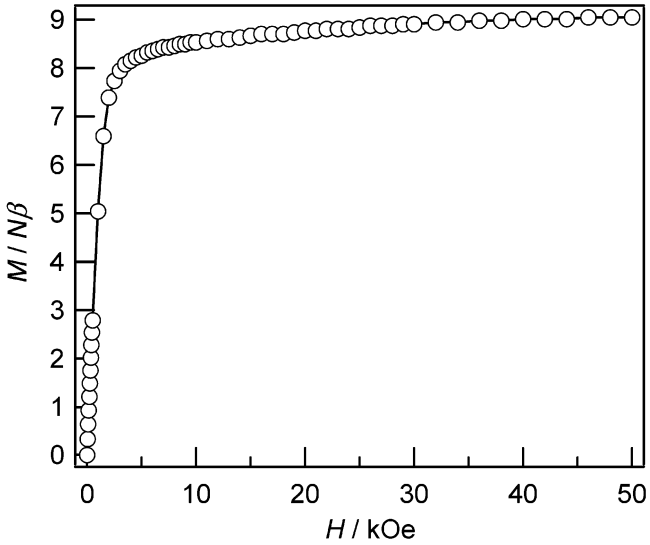

Figure 9. Field dependence of magnetization of complex **2**.

in zero overlap integral and lead to the ferromagnetic interaction between Mn^{II} and W^V, i.e., J_{12}, $J_{13} > 0$. In contrast, the d_{z^2} orbital of W^V and the $d_{x'y'}$, $d_{z'^2}$ and $d_{x'^2} - y'^2$ orbitals of Mn^{II} give the nonzero overlap integral, leading to the antiferromagnetic interaction between Mn^{II} and W^V, J_{11}, J_{14}, and $J_{15} < 0$ (Scheme 2). According to the angular overlap model, the strongest antiferromagnetic contribution comes from the pathway with $d_{z^2}-d_{x'y'}$, $J_{11} \ll J_{14}$, $J_{15} < 0$. This is because a preferential direction the angle between the z axis and the W−CN−Mn linkage (57.4°) allows the π mode of overlap between the $\pi(p_{y'}-p_{y'})$ orbital of CN group and the d_{z^2} orbital of W^V.[27] This angle meanwhile gives rise to the very weak interaction by the pathway of $d_{z^2}-d_{z'^2}$ and

(24) Perumareddi, J. R.; Liehr, A. D.; Adamson, A. W. *J. Am. Chem. Soc.* **1963**, *85*, 249.
(25) Parish, R. V.; Perkins, P. G. *J. Chem. Soc. A* **1967**, 345.
(26) The molecular orbital energy levels and symmetrical modes of $W^V(CN)_8$ in ref 22 are used here, and those of $Mn^{II}(NC)_4O_2$ were calculated by the DV-Xα method, assuming that both Mn−O bonds are equivalent and the Mn ion is coplanar with the four CN groups. The absolute values of the energy levels (E and E') were not given, i.e., Mn and W in Schemes 2 and 3 do not have the same energy level coordinate.

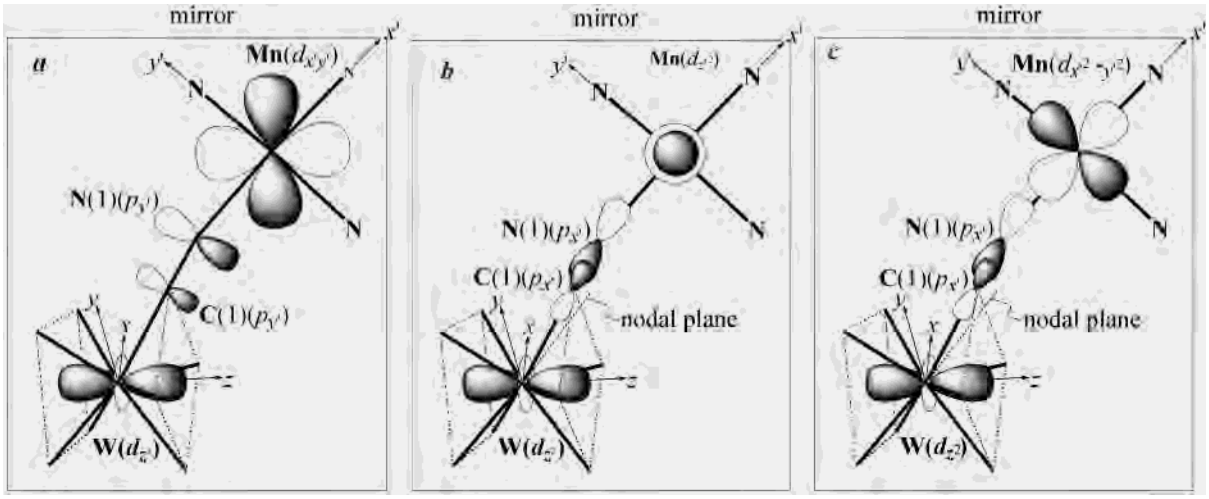

Figure 10. Superexchange pathways of J_{11} (*a*), J_{14}, (*b*) and J_{15} (*c*). *x*′, *y*′, and *z* axes in the mirror plane.

Scheme 2

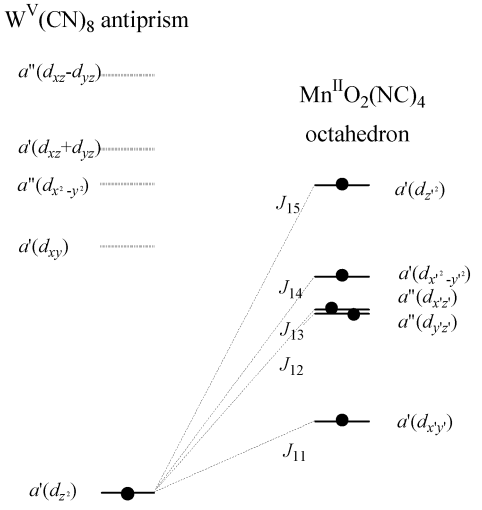

Scheme 3

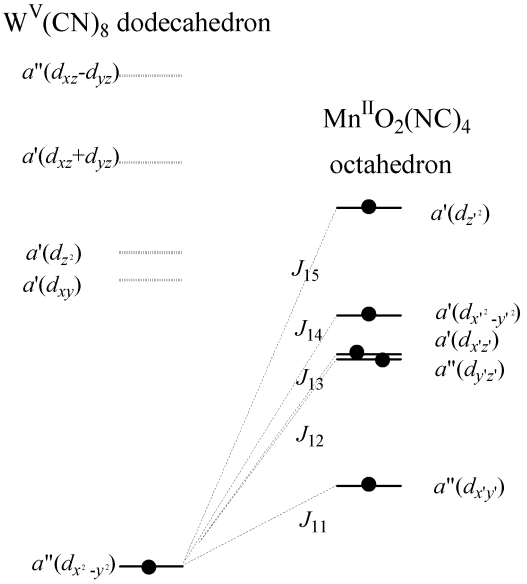

$d_{z^2}-d_{x^2-y^2}$ despite the participation of CN orbitals. Thus, the J_{11} pathway dominates the ferrimagnetic behavior of complex **1**.

For complex **2**, there are two configurations of $W^V(CN)_8$. The same analysis as that in complex **1** is available to the molecular orbitals in complex **2** for the part involving square antiprism. The molecular orbital energy levels and symmetrical modes for the part involving dodecahedron are shown in Scheme 3.[24−26] The coordinates for $Mn(NC)_4O_2$ are determined using the square antiprism geometry, but in new molecular $O_2(CN)_3Mn-NC-W(2)(CN)_7$ the symmetries of $d_{x'y'}$ and $d_{x'z'}$ for Mn^{II} ion will be changed by the new symmetrical operation. The two main superexchange pathways among the occupied molecular orbitals are drawn in Figure 11. In complex **2**, the $d_{x^2-y^2}$ of W^V is the magnetic orbital and forms the five exchange pathways with the five Mn^{II} orbitals. The ferromagnetic superexchange pathways of J_{13}, J_{14}, and J_{15} are created from the nonoverlapped interaction of $d_{x^2-y^2}$ of W^V and $d_{x'z'}$, d_{z^2} and $d_{x'^2-y'^2}$ orbitals of Mn^{II}, respectively. The other two orbitals of Mn^{II} possess the same symmetry as $d_{x^2-y^2}$ of W^V and give rise to the antiferromagnetic contributions. J_{11} is the pathway with the largest overlap of $d_{x^2-y^2}$ of W^V and $d_{x'y'}$ of Mn^{II} through the cyano-bridge orbitals. The *xy* plane with the orbital from W^V crosses the plane with the $p_{y'}-\pi$ orbital of the cyano-bridge and $d_{x'y'}$ at 16.2°. This causes a slight reduction in the orbital overlap but is still a significant antiferromagnetic contributor. The angle, however, allows a contribution from the J_{12} magnetic pathway, which arises from the overlap of the $d_{x'z'}$ orbital of Mn^{II} and the $d_{x^2-y^2}$ of W^V, despite the absence of the cyano-ridged orbitals. Thus, $J_{11} \ll J_{12} < 0$.

When comparing the magnetic exchange pathways between W^V and Mn^{II} in the two magnets, it is easy to understand why their magnetic properties are similar. The strongest exchange pathway dominates the properties, and there is only one strong exchange pathway between either the square antiprismatic or the dodecahedral $W^V(CN)_8$ and

(27) In the angle distribution diagram of the d_{z^2} wave function, the value from the origin to the boundary surface belonging to the *z*-axis is twice that in the *xy* plane. Thus, the line formed by connecting the boundary points on the *x* and *z* axes in the $W(d_{z^2})$ diagram is almost parallel with the $C(1)(p_{y'})$ orbital, because the angle is 96.0° (= 180° − 57.4° − ($\tan^{-1}$ 0.5)°) between the line and the W−CN−Mn linkage. Therefore, the orbitals of $W(d_{z^2})$ and $C(1)(p_{y'})$ can have the largest overlap in this direction.

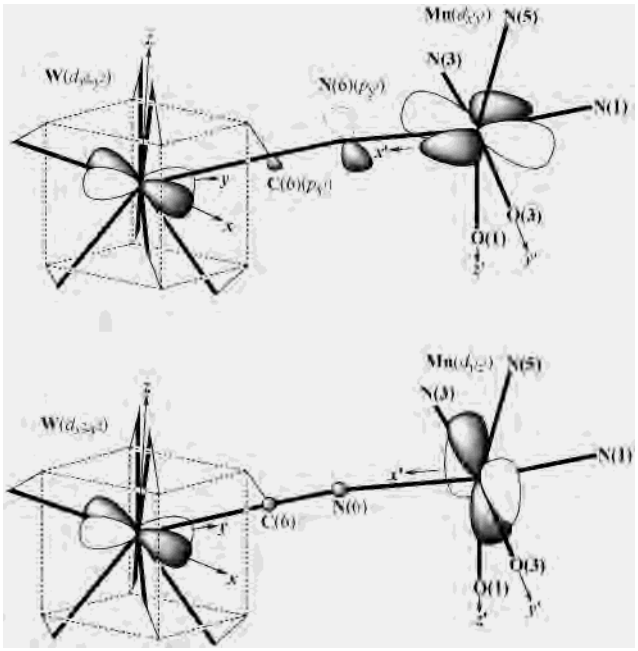

Figure 11. x', z', and z axes in the mirror plane.

the octahedral $Mn(NC)_4O_2$, i.e., the π-like orbital interaction that Mn ion provides d_{xy} orbital with the participation of the p$-\pi$ orbital of the cyano bridge.

In complexes **1** and **2**, the Curie temperatures were higher than those of the Prussian blue analogues with the same spins such as $Mn^{II}_{1.5}[Fe^{III}(CN)_6]\cdot 12H_2O$ ($T_c = 9$ K).[28] To further understand the magnitude of the magnetic coupling between Mn^{II} and W^{V} ions, the J values have been estimated. J_{MnW} and J_{MnFe} can be obained by eq 3:

$$T_C = \frac{2(Z_{M_A}Z_{M_B})^{1/2}|J_{M_AM_B}|(S_{M_A}(S_{M_A}+1)S_{M_B}(S_{M_B}+1))^{1/2}}{3k} \quad (3)$$

where Z_M is the number of the nearest neighbors bridged to M ($Z_{Fe} = 6$, $Z_{Mn} = 4$ for $Mn^{II}-Fe^{III}$, $Z_W = 8$ and $Z_{Mn} = 4$ for **1** and **2**, respectively) and k is the Boltzmann constant, 0.69372 $cm^{-1}\,K^{-1}$. The exchange coupling constants between the M_A and M_B ions, $J_{M_AM_B}$, are $J_{MnFe} = -0.75$ cm^{-1} for $Mn^{II}-Fe^{III}$, $J_{MnW} = -2.9$ cm^{-1} for **1**, and -3.2 cm^{-1} for **2**, respectively. Besides the contribution of Z_M to T_C, the $J_{M_AM_B}$ values show that the magnetic orbital couplings in **1** and **2** are stronger than that in $Mn^{II}-Fe^{III}$, even though the orbital overlap between $W^{V}(CN)_8$ and Mn^{II} ions is not along the most advantageous spatial orientation. This indicates that other factors dominate the magnetic exchange interaction in the octacyanotungstate system. One possible factor is the large diffusion of the 5d orbitals in the tungstate ions. Tungsten has a large ionic radius, and the electron density of 5d orbitals is usually near $30a_0$ (a_0: Bohr radius) from the nucleus, but the highest electron density of a 3d orbital is typically less than $7a_0$. Therefore, the magnetic orbitals of W^{V} ions overlap with neighboring metal ions through cyano group over a larger space.

In conclusion, two new cyano-bridged tungstate(V)−manganese(II) bimetallic complexes were successfully synthesized in aqueous acetic acid and were characterized structurally. Both complexes revealed three-dimensional networks, but they contained the different geometries of the $[W(CN)_8]^{3-}$ building unit attributed to the reaction conditions. This indicates that it was possible not only to control the crystal growth but also to vary the coordination geometry around the W^{V} ion to either square antiprismatic or dodecahedral by modulating the concentration of acetic acid. The investigation on the magnetic properties showed that the difference in structure led to the different superexchange pathways dominating the ferrimagnetic ordering in **1** and **2**. So, the synthetic strategy reported here provides an example in coordination synthesis methodology on the design and preparation of new functionallized molecule-based magnets from $[W(CN)_8]^{3-}$ building blocks, which possess useful physical properties.

Acknowledgment. We thank Japan Science and Technology Corporation (JST) for financial support. S.Y. is an STA postdoctoral fellow (ID No. 200107).

Supporting Information Available: Two X-ray crystallographic files in CIF format and two figures in χ_M-T, $\mu_{eff}-T$ for **1** and **2**. This material is available free of charge via the Internet at http://pubs.acs.org.

IC025959X

(28) Gadet, V.; Bujoli-Doeuff, M.; Force, L.; Verdaguer, M.; Malkhi, K. E.; Deroy, A.; Besse, J. P.; Chappert, C.; Veillet, P.; Renard, J. P.; Beauvillain, P. *Magnetic Molecular Materials*; Gatteschi, D., Kahn, O., Miller, J. S., Palacio, F., Eds.; NATO ASI Series E.; Plenum: New York, 1991; Vol. 198.